



Neotectonics of the central Nepalese Himalaya: Constraints from geomorphology, detrital $^{40}\text{Ar}/^{39}\text{Ar}$ thermochronology, and thermal modeling

Cameron W. Wobus,^{1,2} Kelin X. Whipple,¹ and Kip V. Hodges¹

Received 12 December 2005; revised 21 April 2006; accepted 28 April 2006; published 29 July 2006.

[1] The southern flanks of the central Nepalese Himalaya correspond to a sharp transition in landscape morphology and bedrock mineral cooling ages that suggests a change in rock uplift rate. This transition can be explained by either (1) accretion of footwall material to the hanging wall across a ramp in the décollement separating India from Eurasia, thereby enhancing rock uplift rates above the zone of accretion or (2) out-of-sequence surface thrust faulting at the physiographic transition. Here we use geomorphic data, 649 new detrital $^{40}\text{Ar}/^{39}\text{Ar}$ cooling ages, and a simple thermokinematic model to evaluate which of these tectonic configurations is most appropriate for the central Nepalese Himalaya. We first define and delineate the physiographic transition in central Nepal using maps of knickpoints, river steepness indices, local relief, and the distribution of thick alluvial fill deposits. We then report new detrital $^{40}\text{Ar}/^{39}\text{Ar}$ data from two trans-Himalayan transects, each of which suggests a rapid northward increase in the total amount of exhumation across the physiographic transition. Thermokinematic modeling suggests that either of the two developmental scenarios for the transition is plausible but that an accretion model is viable only under an extremely narrow range of conditions. We contend that the physiographic and thermochronologic data in our study area are most simply explained by recent out-of-sequence surface thrusting within the Lesser Himalayan metasedimentary sequence, approximately 15–30 km south of the mapped surface trace of the Main Central Thrust system. An important finding of this work is that there are substantial along-strike variations in physiography and thermal history that reflect along-strike changes in the degree and location of out-of-sequence surface thrusting. **Citation:** Wobus, C. W., K. X. Whipple, and K. V. Hodges (2006), Neotectonics of the central Nepalese Himalaya: Constraints from geomorphology, detrital $^{40}\text{Ar}/^{39}\text{Ar}$

thermochronology, and thermal modeling, *Tectonics*, 25, TC4011, doi:10.1029/2005TC001935.

1. Introduction

1.1. Motivation

[2] As a textbook example of continent-continent collision, the Himalaya provides an excellent natural laboratory to study the tectonic architecture of an evolving orogenic system. Over the past decade, a wealth of new data have been published allowing refined estimates of exhumation rates and pressure-temperature paths along local transects across the range [Copeland *et al.*, 1991; Vannay and Hodges, 1996; Harrison *et al.*, 1997; Catlos *et al.*, 2001; Kohn *et al.*, 2001; Brewer *et al.*, 2003; Burbank *et al.*, 2003; Bollinger *et al.*, 2004; Vannay *et al.*, 2004; Hodges *et al.*, 2005; Ruhl and Hodges, 2005; Viskupic *et al.*, 2005]. However, while each new data set helps constrain viable tectonic models of Himalayan evolution [Beaumont *et al.*, 2004; Jamieson *et al.*, 2004], extrapolating surface observations to the architecture of the subsurface leaves ample room for interpretation.

[3] In the central Nepalese Himalaya, several tectonic models have been proposed to explain an observed break in rock uplift rate across a dramatic physiographic transition between the high Himalayan ranges and their foothills [Cattin and Avouac, 2000; DeCelles *et al.*, 2001; Wobus *et al.*, 2005]. Each of these models implies a different degree of exhumation at the foot of the high range, and therefore each suggests a different degree of importance for surface processes in driving this exhumation. As a result, the differences in the details of these models may lead to varying interpretations of how closely climate and tectonics may be coupled in the Himalaya [Beaumont *et al.*, 2001; Burbank *et al.*, 2003; Molnar, 2003; Hodges *et al.*, 2004; Wobus *et al.*, 2005].

1.2. Approach and Scope

[4] Our approach to understanding the tectonics of the central Nepalese Himalaya involves three major avenues of inquiry. We begin with an analysis of landscape morphology in central Nepal, with the assumption that changes in physiography can be used to characterize the distribution of rock uplift rates, and therefore the locus of active deformation, across the range front [Snyder *et al.*, 2000; Wobus *et al.*, 2006]. This analysis builds on previous work [Seeber and Gornitz, 1983; Hodges *et al.*, 2001; Wobus *et al.*, 2003;

¹Department of Earth, Atmospheric and Planetary Sciences, Massachusetts Institute of Technology, Cambridge, Massachusetts, USA.

²Now at Cooperative Institute for Research in Environmental Sciences, University of Colorado, Boulder, Colorado, USA.

Hodges et al., 2004; *Wobus et al.*, 2005] which has identified and characterized a prominent morphologic break in central Nepal, hereafter referred to as physiographic transition 2, or PT₂. Our first goal is to examine the nature and position of this physiographic transition and its relation to mapped structures. This physiographic characterization then provides a framework for interpreting regional patterns in thermochronologic data, for examining the likelihood of significant variability in the tectonic architecture of central Nepal, and for evaluating alternative tectonic models for the evolution of the range.

[5] We supplement our analysis of landscape morphology with new detrital ⁴⁰Ar/³⁹Ar cooling-age data from two transects in central Nepal. These ⁴⁰Ar/³⁹Ar cooling ages provide a means of characterizing the exhumation history of rocks between middle crustal positions (~350°C) and the surface. Samples are derived from small tributaries to the Trisuli and Bhothe Kosi rivers, and each set of samples represents a strike-normal transect of approximately 50 km across PT₂. In conjunction with published detrital ⁴⁰Ar/³⁹Ar data from the Burhi Gandaki river [*Wobus et al.*, 2003], these data characterize cooling ages across the physiographic transition for nearly 100 km along strike. We note how our data and other published results [e.g., *Bollinger et al.*, 2004] provide evidence for along-strike variations in the bedrock exhumation histories of rocks on either side of PT₂ in central Nepal.

[6] Our geomorphic and thermochronologic data can be explained easily by persistent, active thrusting at PT₂ over much of the middle Miocene-Recent interval [*Wobus et al.*, 2003, 2005]. However, recent work by *Bollinger et al.* [2004, 2006] suggests that such observations might also be explained by erosional exhumation of a thrust duplex formed by accretion of material from the downgoing Indian Plate across a buried thrust ramp with no surface faulting. To test this hypothesis, we explore a simple thermokinematic model for the tectonic evolution of central Nepal which allows us to evaluate the range of structural geometries that can produce the observed pattern of ⁴⁰Ar/³⁹Ar ages from our detrital samples. If the kinematics assumed by *Bollinger et al.* [2004, 2006] are correct, our modeling suggests that only a very narrow range of parameters can produce the observed distribution of cooling ages in central Nepal for a given midcrustal ramp geometry.

2. Background

[7] It has been known for more than a half century that the structural geometry of the Himalaya is dominated by three major south vergent thrust systems [*Heim and Gansser*, 1939]. From north to south, they are the Main

Central Thrust (MCT), the Main Boundary Thrust (MBT), and the Main Frontal Thrust (MFT) systems (Figure 1). The MCT system places high-grade schists, gneisses, and migmatites of the Greater Himalayan Sequence (GHS) atop amphibolite-greenschist facies phyllites and psammites of the Lesser Himalayan Sequence (LHS). This structural configuration gives rise to the well-known “inverted metamorphism” in the Nepalese Himalaya, in which metamorphic grade increases up section through the Lesser Himalayan rocks and into the footwall of the MCT system [e.g., *Arita*, 1983; *Harrison et al.*, 1998] (Figure 1c). Farther south, the LHS is thrust over unmetamorphosed molassic strata along the MBT system, and these “Subhimalayan” units are, in turn, thrust over the undeformed Gangetic Plains on the Main Frontal Thrust system [*Hodges*, 2000]. Most researchers agree that all three of these thrust systems probably root at depth into a basal décollement typically referred to as the Himalayan Sole Thrust (HST) [*Schelling and Arita*, 1991; *Hauck et al.*, 1998].

[8] Seismic reflection profiles in southern Tibet [*Zhao et al.*, 1993] have identified the HST at a deeper level than would be expected from simple downdip projections of the shallow dip of the HST beneath the Himalayan foreland [*Schelling and Arita*, 1991]. This observation supports the interpretation of *Lyon-Caen and Molnar* [1983] that a large ramp in the HST lies just below PT₂ (Figure 2a). Subsequent workers [*Pandey et al.*, 1995; *Cattin and Avouac*, 2000; *Cattin et al.*, 2001; *Avouac*, 2003] have sought to refine models of the geometry and position of this ramp using a variety of geophysical data sets. The inferred ramp flat geometry has been used to explain changes in surface uplift rates between the foothills and the high Himalayas over interseismic timescales [*Jackson and Bilham*, 1994; *Bilham et al.*, 1997], as well as the existence of PT₂ over Holocene timescales [*Lave and Avouac*, 2001]. If these explanations are extended to longer timescales, however, the implied kinematics in the hanging wall of the HST ramp are inconsistent with the unreset ⁴⁰Ar/³⁹Ar cooling ages observed by *Copeland et al.* [1991] and *Wobus et al.* [2003] near PT₂ in central Nepal. In particular, without either accretion [e.g., *Bollinger et al.*, 2006] or surface thrusting [e.g., *Wobus et al.*, 2003], the particle paths predicted for the hanging wall of the HST for even modest overthrusting velocities (≤ 5 mm yr⁻¹) would bring reset rocks to the surface in ~10 Myr.

[9] The tectonic stratigraphy of the Himalaya is complicated in central Nepal by the presence of the Kathmandu allochthon, an ~100 km wide exposure of amphibolite-facies metamorphic rocks and granitic intrusions that is preserved in the core of a broad synform overlying less metamorphosed LHS units (Figure 1c). On the southern

Figure 1. Study area and generalized tectonic and geomorphic setting. (a) Regional map showing location of study area in the Himalayan system. PAK, Pakistan; NEP, Nepal; BHU, Bhutan; BAN, Bangladesh; MYR, Myanmar. (b) Major tectonic structures and river systems. MAR, Marsyandi river; BG, Burhi Gandaki river; TR, Trisuli river; IN, Indrawati river; BK, Bhothe Kosi river; STF, South Tibetan fault. All other abbreviations are as in text. A-A' indicates location of schematic cross sections in Figure 2. Grey box indicates location of Figures 1c, 3, and 5. (c) Generalized geology of the study area, compiled from *Colchen et al.* [1986], *Shrestha et al.* [1987], and *Johnson et al.* [2001]. Thick dashed grey lines show approximate position of biotite (BIO) and garnet (GRT) isograds from *Colchen et al.* [1986].

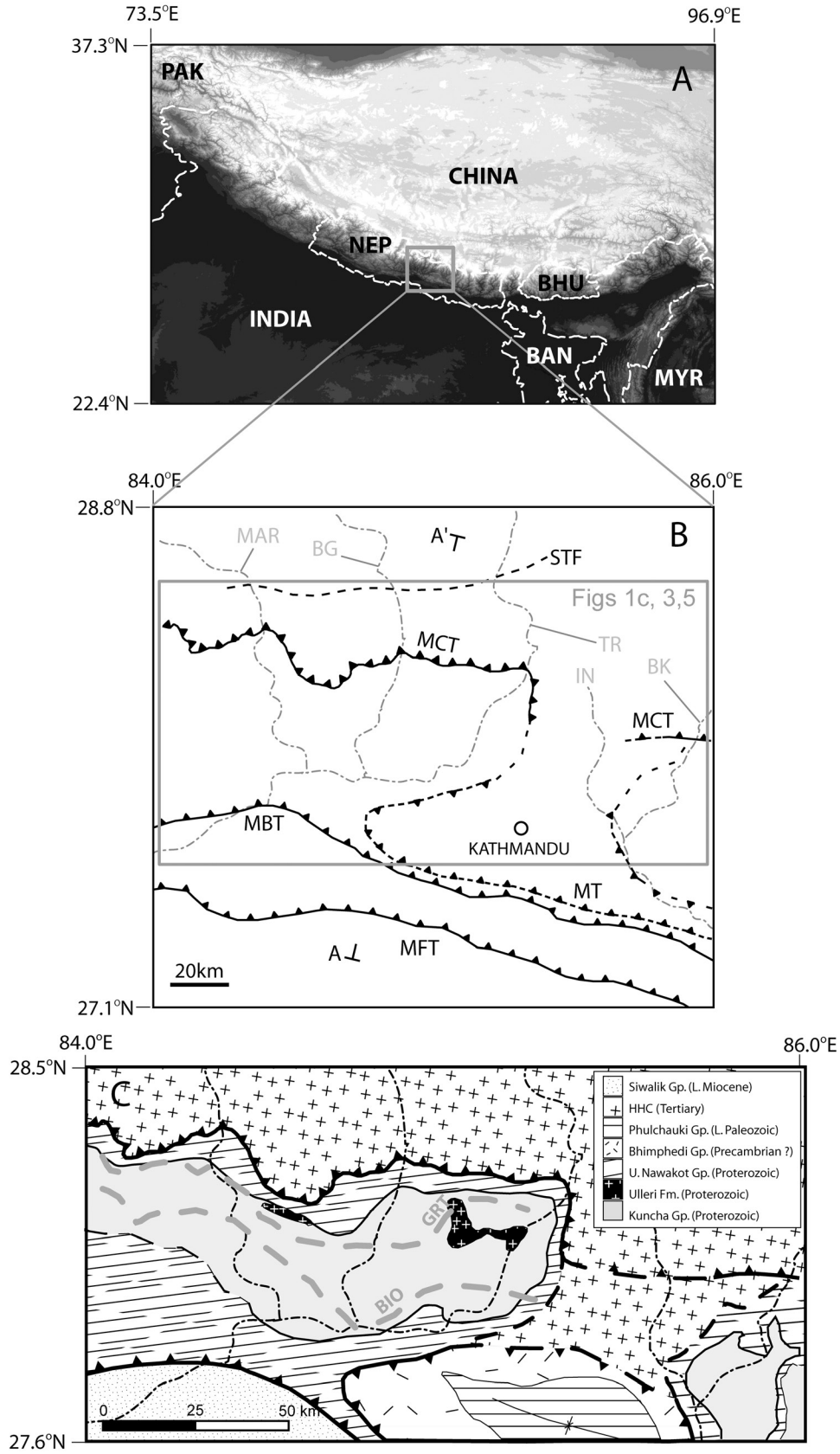


Figure 1

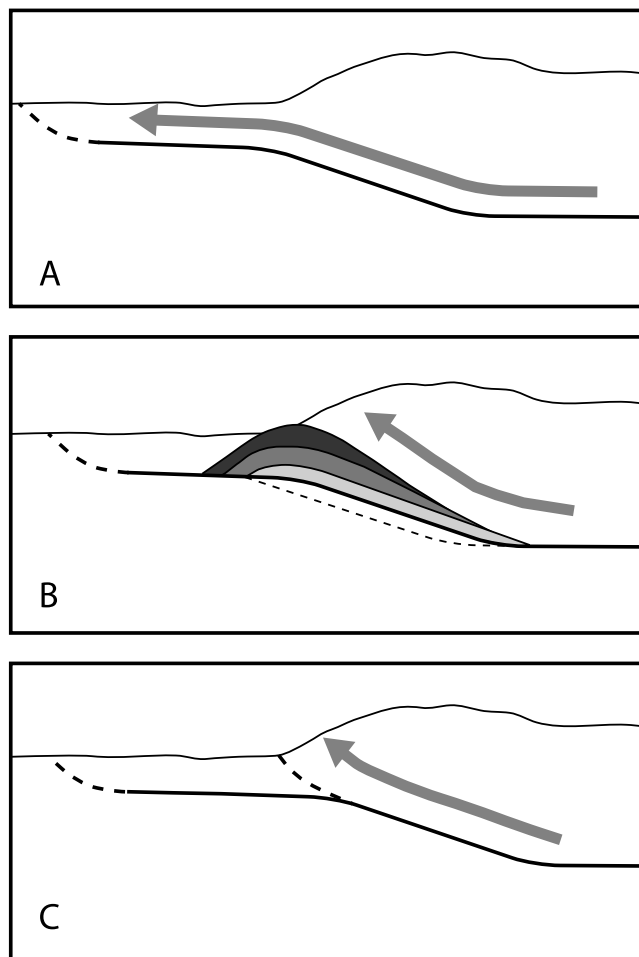


Figure 2. Simplified diagrams showing three viable models for neotectonics in central Nepal, with hanging wall particle trajectories illustrated schematically. (a) Surface thrusting is concentrated at the MFT. The change in rock uplift rates at the physiographic transition results from a passively deforming hanging wall as material is transported over the ramp in the MHT [e.g., *Cattin and Avouac*, 2000; *Lave and Avouac*, 2001]. (b) Surface thrusting remains concentrated at the MFT, with rock uplift rates at the physiographic transition augmented by accretion of material from the footwall to the hanging wall [e.g., *Bollinger et al.*, 2004]. Hanging wall deformation is accommodated along foliation-parallel slip planes above the accretion zone. (c) Active thrusting occurs at the physiographic transition. The break in rock uplift rates and the position of the physiographic transition result from differential motion along this fault [e.g., *Wobus et al.*, 2003, 2005].

flank of the synform, the allochthon is separated from underlying rocks by the north dipping Mahabarat Thrust (MT). Some workers [e.g., *Stöcklin*, 1980] regard the MT as a southward extension of the Main Central Thrust system, making the Kathmandu allochthon a half klippe of Greater Himalayan Sequence rocks. Unfortunately, exposures of the

northern flank of the synform are very poor, and a variety of structural relationships between the allochthon and the GHS have been proposed [e.g., *Stöcklin*, 1980; *Rai et al.*, 1998; *Upreti and Le Fort*, 1999; *Johnson et al.*, 2001; *Rai*, 2001]. Although basal units of the Kathmandu allochthon are, in some places, similar to GHS units, the precise relationship between the Mahabarat Thrust and the Main Central Thrust system remains unclear [*Hodges*, 2000; *Gehrels et al.*, 2003]. Our compilations shown in Figures 1b and 1c depict the uncertainty in this region [*Johnson et al.*, 2001], as well as the position of major structures farther to the south and west where geologic mapping has been more comprehensive [*Stöcklin*, 1980; *Colchen et al.*, 1986; *Shrestha et al.*, 1987].

[10] The folding of the Kathmandu allochthon and structural mapping from western and central Nepal suggest at least some degree of thrust duplexing along the HST ramp at depth. Recent cross sections through western and central Nepal, for example, include a crustal-scale structure commonly referred to as the “Lesser Himalayan Duplex”, which is proposed to date to the middle Miocene [*DeCelles et al.*, 2001; *Robinson et al.*, 2003]. *Bollinger et al.* [2004, 2006] have suggested that duplexing at depth may be a quasi-steady state process, continuing throughout much of the past 20 Myr (Figure 2b). This “steady state accretion” model suggests that the ramp in the HST propagates southward with time, abandoning a succession of blind thrust faults in the hanging wall. An important kinematic requirement of the *Bollinger et al.* [2004, 2006] model is that the hanging wall continues to deform during ramp propagation by incremental slip along a penetrative set of foliation-parallel shear zones. This penetrative deformation suggests that hanging wall rocks should record smooth gradients in the total depth of exhumation from south to north. Under the right set of geometric conditions, such an accretion model should also be capable of producing a break from reset to unreset $^{40}\text{Ar}/^{39}\text{Ar}$ cooling ages within the Lesser Himalayan Sequence, since the kinematics require at least some of the footwall rocks accreted to the hanging wall to be reexhumed before reaching the depth of the closure isotherm for $^{40}\text{Ar}/^{39}\text{Ar}$ [*Bollinger et al.*, 2006]. One of the goals of our thermal and kinematic modeling is to evaluate the range of structural geometries that might create such a break in cooling ages.

[11] A final class of models suggests that new thrust faults break to the surface near the updip projection of the inferred HST ramp. This geometry is supported by geochronologic data from central Nepal, which suggest Pliocene synkinematic metamorphism of rocks within and in the immediate footwall of the Main Central Thrust system, long after the canonical Miocene age of MCT deformation [*Harrison et al.*, 1997; *Catlos et al.*, 2001; *Kohn et al.*, 2001]. In addition, discontinuities in $^{40}\text{Ar}/^{39}\text{Ar}$ and fission track age patterns across the physiographic transition [*Copeland et al.*, 1991; *Wobus et al.*, 2003; *Huntington and Hodges*, 2006], a sharp discontinuity in surface erosion rates constrained by cosmogenic isotopes [*Wobus et al.*, 2005], and the presence of young brittle deformation in the vicinity of the MCT system [*Hodges et al.*, 2004] are most

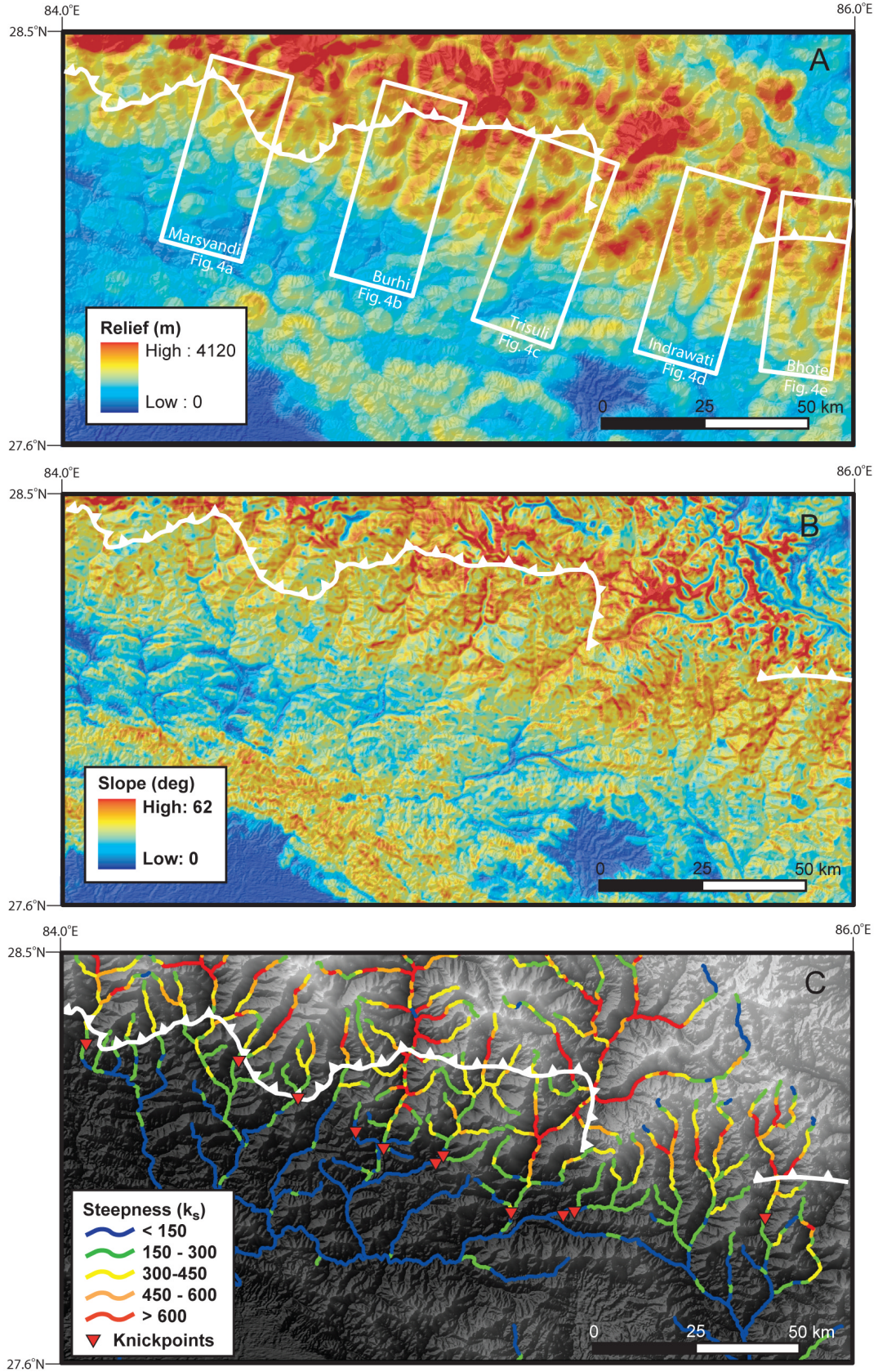


Figure 3

easily explained by a model of sustained or episodic exhumation along surface-breaking thrusts near PT₂ (Figure 2c).

3. Geomorphology

[12] Since rock uplift is ultimately the engine driving relief production in active orogens, the geomorphology of the Himalaya should provide some constraints on the distribution of rock uplift rates through central Nepal. With this in mind, one of the more enigmatic characteristics of the central Nepalese Himalaya is the existence of PT₂ nearly 100 km north of the Himalayan thrust front [Seeber and Gornitz, 1983]. Previous work has described the distribution of potential energy, hillslope gradients and channel steepness indices for portions of central Nepal, all of which suggest that PT₂ may be a morphologic signature of surface thrust faulting at the base of the high range [Hodges *et al.*, 2001; Wobus *et al.*, 2003; Hodges *et al.*, 2004; Wobus *et al.*, 2006]. Here we refine those studies in order to better resolve the nature of PT₂ and its variability along strike in the central Himalaya.

[13] Our geomorphic analyses are derived from a 90-m resolution digital elevation model (DEM) of central Nepal (see Fielding *et al.* [1994] for a description of the data set). The physiographic metrics we employ include local relief calculated over a 2.5-km radius circular window (Figure 3a), hillslope gradients calculated over an ~250 m square and smoothed with a 500 m radius window (Figure 3b), and major knickpoints and normalized steepness indices for trans-Himalayan rivers and their tributaries in central Nepal (Figure 3c). As shown in Figure 3, all three of these measures of physiography show a pronounced discontinuity across central Nepal, whose position broadly corresponds to the surface trace of the MCT system in the western portion of the study area and diverges from the MCT system to the east.

[14] Knickpoints are defined in this study as the downstream limit of high-concavity zones, where channel gradients increase abruptly from south to north. As such, these knickpoints may mark the southern limit of a zone of increasing rock uplift rates [Kirby and Whipple, 2001]. Normalized steepness indices (k_{sn}) are measures of the local channel gradient normalized to the contributing drainage area, and have been shown to be correlated with the rate of rock uplift in settings where the tectonics have been independently constrained [Snyder *et al.*, 2000; Kirby and Whipple, 2001; Lague *et al.*, 2003; Wobus *et al.*, 2006]. Using a reference concavity of 0.45 [e.g., Wobus *et al.*, 2006], we calculated normalized steepness indices over a 4-km moving window along each channel, and color-coded channel reaches by their k_{sn} values throughout central

Nepal. The normalized channel steepness indices do not show the step function break at PT₂ that simple models for bedrock channel incision would predict across a discrete fault [e.g., Whipple and Tucker, 1999]. Instead, the ~10–20 km wide transition in channel steepness (Figure 3c, see also Burbank *et al.* [2003]) could reflect (1) a zone of distributed deformation with rock uplift rate increasing steadily to the north; (2) a reduction of channel steepness in the immediate hanging wall of the fault associated with a belt of orographically enhanced precipitation immediately to the north of PT₂ [Whipple and Tucker, 1999; Burbank *et al.*, 2003; Roe *et al.*, 2003; Thiede *et al.*, 2004]; or (3) a downstream blurring of the morphologic signature of a sharp break in rock uplift because these large rivers approach transport-limited conditions [Whipple and Tucker, 2002]. As we have documented elsewhere [e.g., Wobus *et al.*, 2003, 2005], the regionally consistent increase in channel steepness at PT₂ is correlated with changes in channel morphology, bed state, and soil thickness and color. Furthermore, the physiographic transition is not well correlated with lithologic boundaries, and the pattern of hillslope and channel gradients is the opposite of what we would expect from the pattern of orographically enhanced precipitation in the absence of a change in rock uplift rates. Collectively, these observations strongly argue for an increase in rock uplift rate.

[15] In order to pinpoint the positions of changes in rock uplift rates from our geomorphic data, we focus here on delineating the southern limit of the physiographic transition. We define this position as the union of (1) the downstream limit of relatively high (>150 m^{0.9}) steepness indices in tributary valleys; (2) the downstream limit of high-concavity zones in tributary profiles, marked as knickpoints on these channels; (3) the position of an abrupt change in local relief; and (4) the upstream limit of thick terrace fills in trunk and tributary valleys. Note that the use of the southern limit of PT₂ here is consistent with that of Wobus *et al.* [2003, 2005] but differs slightly from that of Hodges *et al.* [2004] in which the upper limit of the physiographic transition was marked instead. These approaches are equivalent when PT₂ is sharp but yield slightly different definitions of PT₂ where the transition is more gradual. As will be shown below, along-strike variations in the sharpness of PT₂ in central Nepal probably reflect changes in the degree of surface deformation along strike.

[16] The position of the physiographic transition is shown in cross-sectional view as vertical shaded bars in Figure 4. Each cross section presents data from a 17–20 km wide swath profile (see Figure 3a), plotting minimum, maximum and mean values of topography and relief, and mean values of hillslope gradient within the swath. These cross sections also show the location of knickpoints, alluvial fill deposits,

Figure 3. Three maps of physiographic data from central Nepal, based on 90-m resolution DEM (see Fielding *et al.* [1994] for description of the data set). (a) Local relief calculated over a circular, 2.5-km radius window. (b) Hillslope gradients, calculated over a 3×3 pixel (~260 m) square window and smoothed with a 500m radius moving average. (c) Map of knickpoints and steepness indices for major river systems of central Nepal and their tributaries (see text for description). In all three maps, white barbed line represents the surface trace of the MCT as defined by Colchen *et al.* [1986], Johnson *et al.* [2001], and Searle *et al.* [1997].

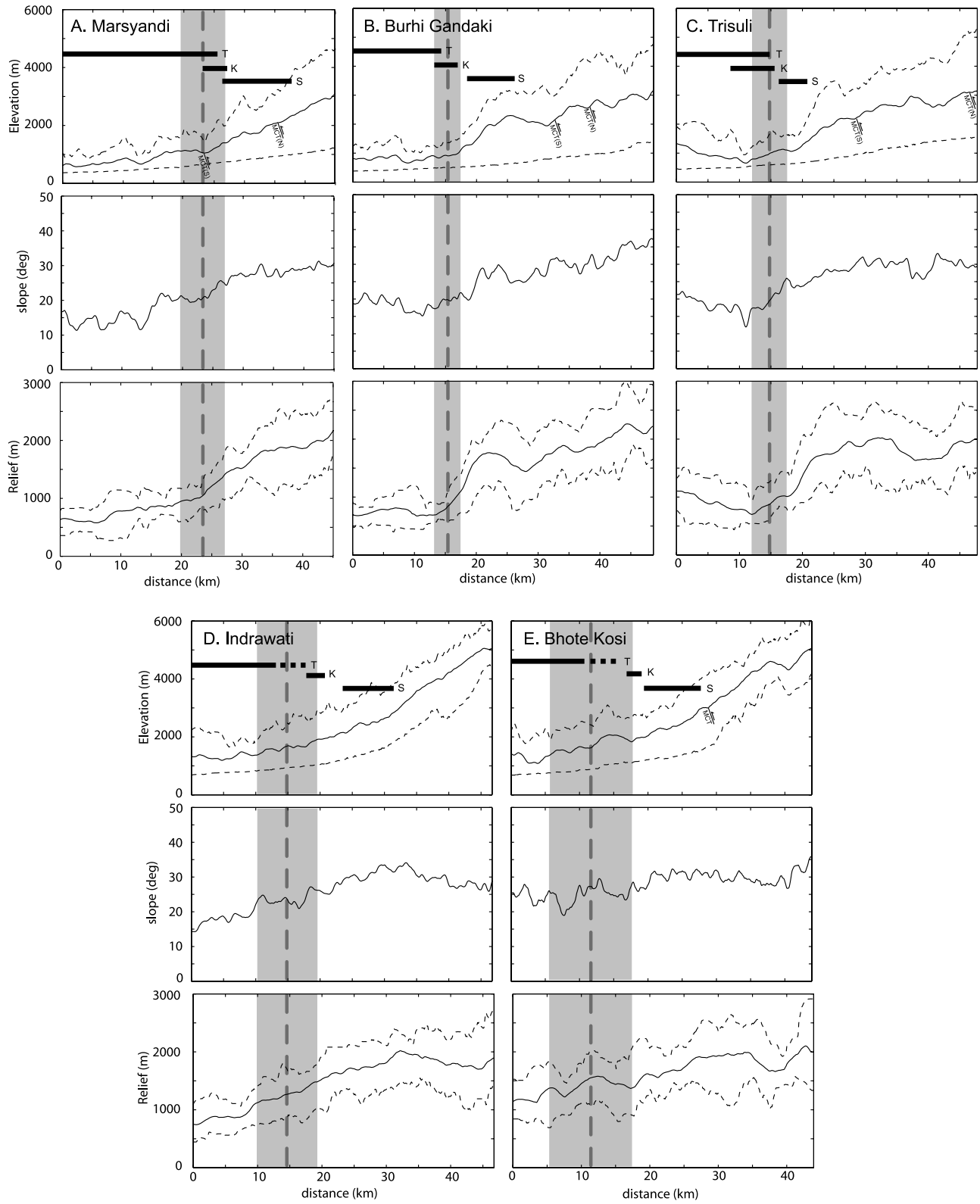


Figure 4

and changes in normalized steepness indices projected onto the midline of each swath. In addition, we indicate the northern and southern projections onto these swaths of the principal strand of the Main Central Thrust system, as defined by *Colchen et al.* [1986] in the west, and *Searle et al.* [1997] and *Johnson et al.* [2001] in the east. We present five swath profiles, following the courses of the Marsyandi, Burhi Gandaki, Trisuli, Indrawati and Bhote Kosi rivers.

[17] At the scale of the entire orogen, PT_2 corresponds closely to the position of the Main Central Thrust system [*Seeber and Gornitz*, 1983; *Hodges et al.*, 2001]. In the Marsyandi valley, the physiographic transition coincides spatially with a zone of deformation that includes faults of the MCT system and other faults within the uppermost Lesser Himalayan sequence rocks, as shown in cross section and map view in Figures 4 and 5 [*Coleman*, 1998; *Martin et al.*, 2005; *Pearson and DeCelles*, 2005]. *Hodges et al.* [2004], and *Huntington and Hodges* [2006] have documented a zone of Quaternary faults near the upper limit of the physiographic transition in this valley, approximately 3–5 km north of the lower limit of PT_2 as shown on Figure 5. Such observations suggest that the relatively broad physiographic transition along the Marsyandi transect may reflect distributed faulting rather than focused, large-magnitude slip on a single out-of-sequence thrust.

[18] The Main Central Thrust system and PT_2 diverge significantly in some parts of the study area, particularly in the lower reaches of the Burhi Gandaki and Trisuli rivers (Figure 5) [e.g., *Wobus et al.*, 2003]. Maps of local relief, hillslope gradients and knickpoints at the downstream limit of tributary steepness transitions highlight an abrupt transition in physiography in these catchments (Figures 3a–3c), while swath profiles illustrate an approximate doubling of relief across only 8–10 km in both the Burhi Gandaki and Trisuli valleys (Figures 4b and 4c). The observed increase in relief is correlated with a south-north disappearance of thick alluvial terraces and valley fills, a clustering of knickpoints along trunk and tributary channels, and the base of a zone of increasing k_s along each of the trunk stream profiles (Figures 3c and 4). Notably, this sharp boundary occurs where the MCT system forms a major reentrant to the north, suggesting that recent tectonic displacements may have activated a new fault that “short cuts” the bend in the MCT system. This hypothesis is corroborated by already published cosmogenic isotope data from the Burhi Gandaki valley, which indicate a fourfold increase in erosion rates

over an across-strike distance of ~2 km that coincides with PT_2 . [*Wobus et al.*, 2005].

[19] To the east in the Indrawati and Bhote Kosi valleys, changes in physiography again occur more gradually than in the Burhi Gandaki and Trisuli valleys, as shown both in map view (Figure 3) and cross-sectional views of topography, relief and hillslope gradients (Figure 4). We know relatively little about the extent of alluvial fill, knickpoints and channel gradients in this eastern part of our study area compared to parts farther west, reflecting both a lack of field observations and a limit to our digital topographic data set. The definition of the physiographic transition in the east is therefore made almost entirely on the basis of steepness indices and large-scale changes in landscape morphology. Nonetheless, the gradual topographic changes in the Indrawati and Bhote Kosi rivers are all suggestive of a more broadly distributed increase in rock uplift rates from south to north, similar to the situation in the Marsyandi valley.

[20] Combining all of our geomorphic observations, the position of the physiographic transition, with estimated uncertainties, is shown in map view on Figure 5. Note that PT_2 narrows and diverges from the MCT system in the Burhi Gandaki and Trisuli rivers, while it widens to the east and to the west. In the west, the physiographic transition and the MCT are nearly coincident. If PT_2 marks a surface-breaking fault, its more gradual expression in the Marsyandi transect suggests that deformation is more distributed where the new fault system incorporates preexisting zones of weakness in the MCT zone or nearby middle Miocene fault systems [*Martin et al.*, 2005; *Pearson and DeCelles*, 2005]. Where the new fault system cuts structurally downward in the preexisting tectonic stratigraphy (i.e., into Lesser Himalayan units of the MCT system footwall), its trace is sharper and, as a consequence, so is PT_2 . We also note that the physiographic transition lies just to the south of an approximate doubling of monsoon precipitation, as documented by *Burbank et al.* [2003]. If this monsoon precipitation record is representative of climate over longer timescales, the resulting erosional unloading may act as a positive feedback that could play an important role in controlling the locus of active thrusting in central Nepal [e.g., *Beaumont et al.*, 2001].

4. Detrital $^{40}\text{Ar}/^{39}\text{Ar}$ Thermochronology

4.1. Previous Work

[21] The muscovite $^{40}\text{Ar}/^{39}\text{Ar}$ thermochronometer provides information about the cooling of rock samples

Figure 4. Swath profiles of topography, slope, and relief along five transects across the range front in central Nepal, arranged from west to east (see Figure 3a for locations). (a) Marsyandi river, (b) Burhi Gandaki river, (c) Trisuli river, (d) Indrawati river, and (e) Bhote Kosi river. In topography and relief plots, dashed lines show minimum and maximum values within the swath; in all swaths, black lines show mean values. Horizontal bars show the position of alluvial fills and terraces (T), knickpoints (K), and zone where steepness indices increase from <300 to $>450 \text{ m}^{0.9}$ in trunk streams (S). Vertical shaded bars and dashed lines show best estimate of PT_2 position based on all available physiographic data. MCT(N) and MCT(S) indicate northern and southern positions of the MCT system within each swath, as defined by *Colchen et al.* [1986], *Johnson et al.* [2001], and *Searle et al.* [1997]. Note that the position of the MCT is debated, particularly along the Indrawati and Bhote Kosi transects [e.g., *Johnson et al.*, 2001].

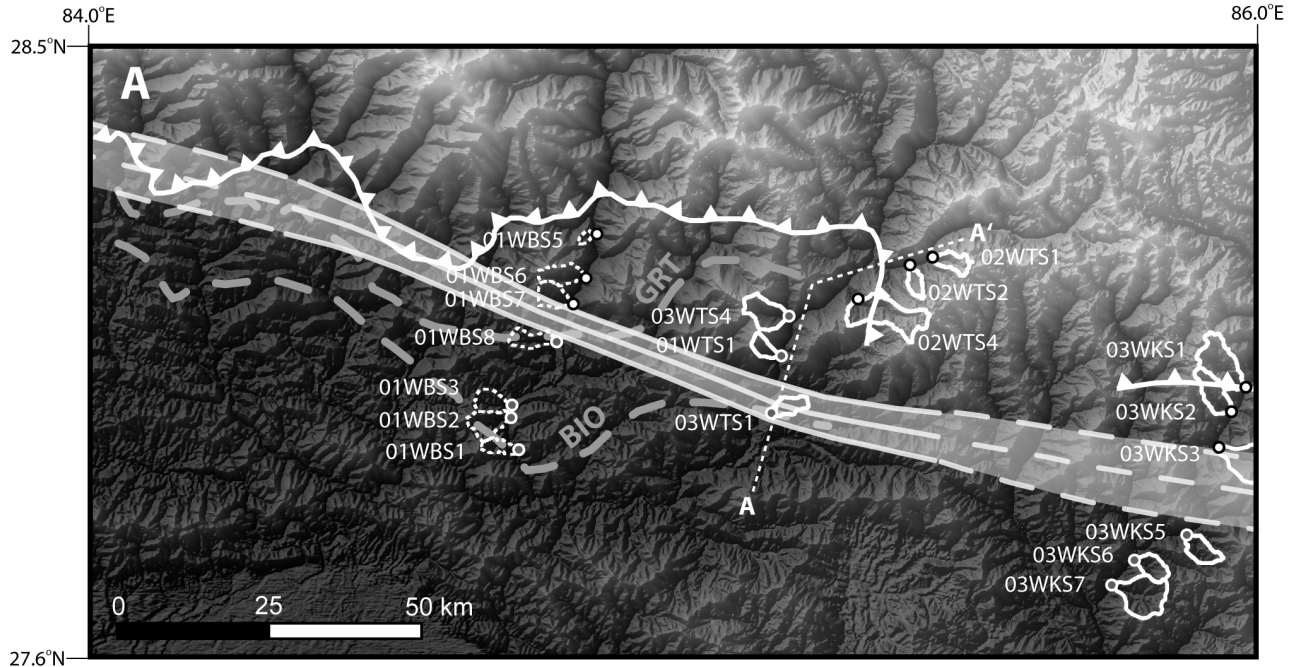


Figure 5. Sediment sample locations and best fit position of PT_2 (see Figures 3 and 4), plotted on a shaded relief map. Dots show sampling locations for $^{40}\text{Ar}/^{39}\text{Ar}$ thermochronology: White dots with black outlines depict samples with Miocene and younger cooling ages; grey dots with white outlines depict samples with Paleozoic and older apparent ages (see Figure 6). White basin outlines show contributing area for each sample. Dashed basin outlines show samples from the Burhi Gandaki river, as previously reported by *Wobus et al.* [2003]. Section line A-A' shows kinked line of projection for Figure 6b. Thick dashed gray lines show approximate position of biotite (BIO) and garnet (GRT) isograds, taken from *Colchen et al.* [1986].

through the $\sim 350^\circ\text{C}$ closure isotherm during exhumation, and thus serves as a useful tool for understanding the midcrustal tectonic architecture of evolving orogenic systems [Hodges, 2003]. In part because of the difficulties in accessing much of the steep topography of the Himalaya, most available bedrock $^{40}\text{Ar}/^{39}\text{Ar}$ dates from central Nepal are confined to widely spaced river valleys and roadways [Copeland et al., 1991; Macfarlane et al., 1992; Edwards, 1995; Bollinger et al., 2004]. In addition, the fine grain size of rocks from the Lesser Himalayan Sequence makes micas difficult to extract from these lithologies, so most data sets focus on coarser rocks of the Greater Himalayan Sequence. Most bedrock cooling ages for samples in central Nepal range from middle Miocene to early Pliocene, with an apparent northward younging from ~ 20 Ma to ~ 3 Ma within the Kathmandu allochthon [Bollinger et al., 2004]. However, a significant number of Proterozoic to early Paleozoic ages have been reported from the Lesser Himalayan Sequence rocks in the Burhi Gandaki drainage and structurally beneath the Kathmandu allochthon farther east [Copeland et al., 1991].

[22] Many of the problems related to poor access and lithology can be eliminated by using detrital thermochronology to characterize the integrated cooling history of complete drainage basins [Hodges et al., 2005]. Recent

detrital $^{40}\text{Ar}/^{39}\text{Ar}$ thermochronologic investigations of modern sediments from central Nepal have begun to provide a more complete picture of cooling ages in the high Himalayas [Brewer et al., 2003; Ruhl and Hodges, 2005], with a distribution of ages that is consistent with the middle Miocene to early Pliocene ages reported for bedrock samples from the same region. Farther to the south, detrital samples from small basins within the Lesser Himalayan Sequence corroborate reports of exceptionally old bedrock cooling ages in the Himalayan foothills [Wobus et al., 2003].

4.2. Methods

[23] The sampling strategy for this study was designed to mimic that of *Wobus et al.* [2003] in the Burhi Gandaki river. Modern river sediments were collected from six tributaries to the Trisuli river and six tributaries to the Bhothe Kosi river, with drainage areas ranging from ~ 9 to 52 km². Because the sampled basins feed large trans-Himalayan trunk streams, they are generally oriented parallel to the structural grain of the orogen and therefore sample small strike-parallel swaths of the landscape (Figure 5). Collectively, the tributary basins for each river system constitute a strike-normal transect that can be used to evaluate changes in cooling history across the range front. Samples were

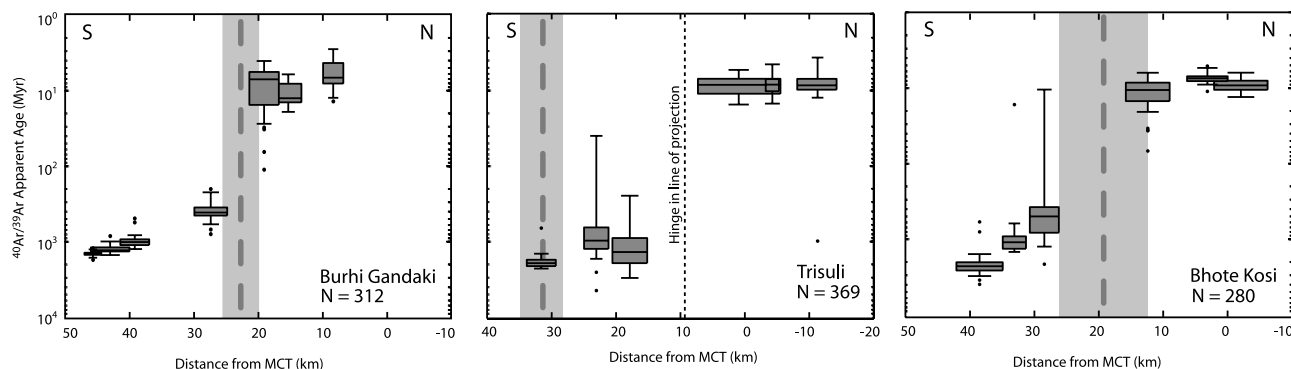


Figure 6. Distribution of $^{40}\text{Ar}/^{39}\text{Ar}$ cooling ages in transects along (a) Burhi Gandaki, (b) Trisuli, and (c) Bhote Kosi rivers, projected onto lines oriented approximately N18°E. In each case, horizontal lines within grey boxes correspond to median ages, upper and lower limits of boxes correspond to 25th and 75th percentiles, and whiskers extend to the limits of the data or 1.5 times the interquartile range (IQR), whichever is smaller. Small dots represent outliers beyond 1.5 times the IQR. Widths of boxes correspond to widths of basins projected onto section line. Dashed vertical lines inside thick grey bands show the location of the physiographic transition in each transect (see Figures 4 and 5). Datum along each transect is taken as the position of the MCT. Note that this position is complicated by the geometry of the MCT system in the Trisuli valley; line of projection is kinked in this profile (see Figure 5).

collected from small bars within the active channels, focusing on the medium to coarse sand size fraction. As in the Burhi Gandaki river, thick fill terraces within the Trisuli and Bhote Kosi trunk stream valleys suggest a period of extensive basin infilling across much of the physiographic Lower Himalaya. In order to avoid contamination of tributary sediments with inputs from these trunk stream terraces, basins with clear evidence of recent infilling were sampled up to 2 km upstream from the tributary mouths. Sample volumes ranged from ~2 to 4 L.

[24] Samples were washed, dried and sieved to remove any organic material and to isolate size fractions for mineral separations. Muscovites were separated using standard mineral separation techniques, focusing on the 500–1000 μm size fraction where possible. In some cases, finer-grained lithologies from the tributary basins required muscovites to be picked instead from the 250–500 μm fraction. In all cases, final mineral separates were picked by hand to ensure sample purity. Following mineral separation, muscovite separates were packaged in aluminum foil and sent to the McMaster University nuclear reactor for irradiation, using Taylor Creek sanidine as a neutron flux monitor (28.34 ± 0.16 Ma [Renne *et al.*, 1998]).

[25] Irradiated muscovite grains were loaded into the vacuum system using stainless steel planchets. Gas was liberated from each sample by total fusion using an Ar ion laser, purified between 5 and 10 min, and analyzed on an MAP 215-50 mass spectrometer with an electron multiplier detector. For each sample, between 50 and 100 single muscovite grains were analyzed. This analytical procedure differs from that of Wobus *et al.* [2003], in which high spectrometer blanks and small grain sizes often required multiple-grain aliquots to be fused for each analysis. The analytical procedure used here ensures that each analysis represents a single grain with a unique cooling history,

rather than a mixture of gas from multiple grains that may have diverse cooling histories. Data were reduced using ArArCalc [Koppers, 2002], with air-corrected blanks. In some cases, high spectrometer blanks or poorly fused samples yielded very low radiogenic ^{40}Ar yields. Analyses reported here are limited to those with radiogenic yields greater than 50%, representing 77% of the samples analyzed from the Trisuli sediments and 96% of the samples analyzed from the Bhote Kosi sediments.

4.3. Results

[26] Both the Trisuli and the Bhote Kosi transects are characterized by a sharp break in $^{40}\text{Ar}/^{39}\text{Ar}$ ages from north to south (Figures 5 and 6). Cooling ages from basins in the north are middle Miocene and younger, while apparent ages from basins in the south are early Proterozoic through Paleozoic (see Table 1 and Tables S1–S12 in the auxiliary material¹). The sharp break in cooling ages from north to south is consistent with thermochronologic data from the Burhi Gandaki valley, which indicate a sharp northward increase in the total depth of exhumation across the physiographic transition [Wobus *et al.*, 2003]. The continuity of this cooling age signal along strike indicates that this northward increase in total exhumation depth is regionally extensive.

[27] Using the break in physiography as a proxy for a break in rock uplift rates, we would predict that discontinuities in cooling ages through central Nepal should coincide exactly with the position of PT₂, which lies along a line oriented slightly south of east between the Burhi Gandaki and Bhote Kosi rivers (Figure 5). As previously docu-

¹Auxiliary materials are available in the HTML. doi:10.1029/2005tc001935.

Table 1. Cooling Ages

Sample	Distance to MCT, km	Drainage Area, km ²	Elevation Range, m	Analyses Reported	⁴⁰ Ar/ ³⁹ Ar Apparent Ages		
					First Quartile	Median	Third Quartile
<i>Trisuli River</i>							
02WTS1	1.1	13.5	3072–5810	60	7.3	8.7	9.9
02WTS2	3.5	8.8	2075–4752	68	7.3	8.5	10.4
02WTS4	10.9	51.8	1821–4951	64	7.2	8.6	11.2
03WTS4	17.1	26	1154–3978	46	879.3	1337.7	1854.4
01WTS1	24	10.1	739–3468	86	637.0	948.7	1204.5
03WTS1	33.6	13.4	626–1656	45	1690.3	1872.3	2043.4
<i>Bhote Kosi River</i>							
03WKS1	0.9	40.3	1729–5422	46	7.9	9.1	10.4
03WKS2	5.1	24	1440–4416	48	6.9	7.4	8.0
03WKS3	11.4	34	1202–3645	49	8.5	10.5	14.6
03WKS5	27	17.4	780–2447	49	362.0	474.9	770.2
03WKS6	33.8	15.5	675–2225 ^a	45	878.5	1037.0	1262.1
03WKS7	38.2	40.8	650–2100 ^a	43	1906.0	2137.4	2426.1
<i>Burhi Gandaki River^b</i>							
01WBS5	7.5	3.4	797–2372	35	4.6	7.0	8.4
01WBS6	15.0	18.4	604–3158	18	8.7	13.1	14.6
01WBS7	19.5	17.5	533–2455	32	5.9	7.4	15.2
01WBS8	26.4	15.6	508–1262	59	356.9	413.0	453.4
01WBS3	38.5	16.7	413–1412	50	929.5	1008.1	1103.5
01WBS2	41.0	22.4	370–1574	58	1163.0	1285.0	1333.2
01WBS1	45.5	10.5	348–1670	60	1392.5	1433.7	1480.7

^aEstimated upper limit (basin extends beyond the range of high-resolution topographic data).

^bPreviously reported analyses [Wobus *et al.*, 2003].

mented, the physiographic transition coincides with the break in cooling ages in the Burhi Gandaki valley [Wobus *et al.*, 2003]. In the Bhote Kosi valley, the break lies directly along the eastward projection of PT₂ (Figures 5 and 6). These observations support a model in which sharp across-strike changes in exhumation history may continue from the Burhi Gandaki eastward across central Nepal. In the Trisuli valley, however, the break in cooling ages lies nearly 15 km north of PT₂ as defined geomorphically, suggesting a more complicated structural configuration than to the east and to the west. The two unreset samples north of PT₂ in the Trisuli valley come from tributaries draining the Ulleri augen gneiss [e.g., Colchen *et al.*, 1986; Shrestha *et al.*, 1987], a cliff-forming orthogneiss whose protolith has a crystallization age of ~1.85 Ga [DeCelles *et al.*, 2000] (see Figure 1c). The unreset ⁴⁰Ar/³⁹Ar cooling ages from this unit, in addition to the northward bend in metamorphic isograds (e.g., Figure 5) suggest that the Ulleri augen gneiss in the Trisuli Valley, in addition to the structurally deeper rocks of the Lesser Himalayan Sequence exposed farther south, has not been buried deeply during Himalayan orogenesis. The rapid transition to Cenozoic ages in rocks exposed north of the Ulleri augen gneiss may be explained by late Miocene-Pliocene (?), out-of-sequence faulting on or near the MCT system trace; however, the lack of a clear geomorphic expression here suggests that this activity has not been recent.

[28] To the south of the outcrop of Ulleri gneiss, the sharp physiographic transition in the Trisuli valley is consistent with an along-strike projection of recent surface faulting from the Burhi Gandaki eastward. The resistant Ulleri augen

gneiss approximately 5 km north of PT₂ may enhance this geomorphic expression, as seen in the high-relief, steep hillslope gradients, and high k_{sm} values in the areas where the Ulleri has been mapped (see Figures 1c and 3). Unfortunately, bedrock exposure is limited in the vicinity of PT₂ and thus we have not been able to test the hypothesis of active faulting there. However, if the transition is indeed structural, such that the Ulleri gneiss is exposed between two out-of-sequence thrust faults of different age, we speculate that such complexity may be related to strong rheologic contrasts between the Ulleri augen gneiss and the surrounding phyllites, and/or to the geometric configuration of the MCT system sidewall ramp along the east side of the Trisuli valley (e.g., Figure 1c) [Macfarlane *et al.*, 1992]. Additional data from low-temperature thermochronometers such as (U-Th)/He apatite, coupled with more detailed structural mapping of the augen gneiss/phyllite contact to the east and west of the Trisuli Valley, would help to resolve this issue.

[29] The transition from young (Miocene) to very old (Paleozoic-Proterozoic) ages in all three transects is a significant finding which requires a discontinuity in cooling history at or near the physiographic transition. However, we note that some of the absolute ages, particularly, the old apparent ages in samples from south of PT₂ and those derived from the Ulleri augen gneiss in the Trisuli valley, are characterized by extremely wide age variability within individual samples and poor precision on individual analyses. This poor data quality is largely a result of an analytical design that was optimized for Miocene samples: As a consequence of this design, the older grains were substan-

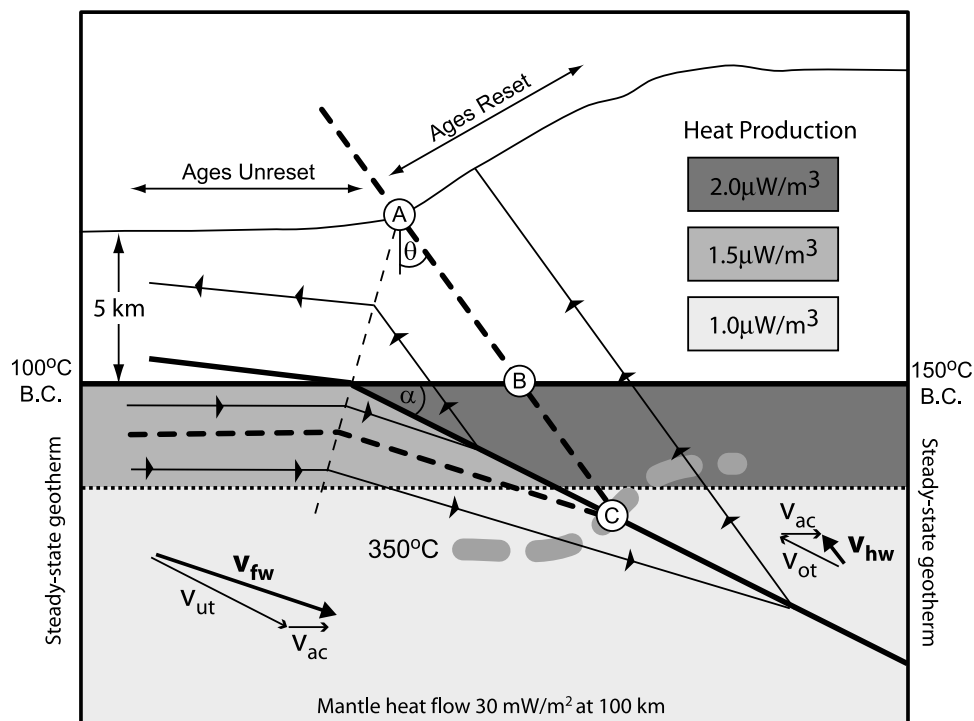


Figure 7. Schematic of model setup and particle paths for continuous accretion across the HST ramp (not to scale). Shaded region depicts the model domain, with the depth of shading corresponding to the assigned heat production in each model segment. Hanging wall particle paths (v_{hw}) are a simple vector sum of the overthrusting rate (v_{ot}) and the accretion rate (v_{ac}). The break in cooling ages at the surface will coincide with the physiographic transition only if the physiographic transition (point A) lies directly along a particle path from the intersection of the closure isotherm and the main décollement (point C). Our simplified model predicts this position at the top of our model domain (point B) using the depth of the décollement beneath the physiographic transition (5 km); the dip of the HST ramp (α); the angle between the hanging wall particle trajectory and the vertical for a given accretion velocity (θ); and the point of intersection between the closure isotherm and the HST ramp, determined from the thermal model.

tially underirradiated. Since the magnitude of the radiogenic ^{40}Ar peak dictates the amount of gas that can be analyzed with the electron multiplier detector without saturating this detector, ^{39}Ar peaks became very small, and the associated measurement error propagates into large age errors. Thus the absolute ages from the south side of the physiographic transition should be viewed with caution. What we can say with confidence, however, is that samples to the south of PT₂, as well as samples 03WTS4 and 01WTS1 on the north side of the transition in the Trisuli drainage, have not experienced significant loss of radiogenic argon during Himalayan orogenesis. This finding places important constraints on the range of thermal histories, and therefore tectonic histories, that these samples have experienced during Himalayan orogenesis.

5. Thermal Modeling

[30] Our thermal modeling was designed to explore the range of tectonic geometries that can produce a change from reset to unreset cooling ages coincident with the change in

rock uplift rate implied by the physiographic transition. The kinematics of our model are defined by the rate of hanging wall overthrusting, the rate of footwall underthrusting, and the rate of accretion of material from the footwall to the hanging wall across the HST ramp [e.g., *Bollinger et al.*, 2006] (Figure 7). Note that as the accretion velocity approaches zero, our model simulates a structural configuration where thrusting is sustained along a discrete fault corresponding to the HST. This scenario can be assumed to replicate either of two end-member cases for the tectonics of central Nepal: If the ramp on the HST is presumed to remain buried and merge with the approximately flat décollement in the physiographic Lower Himalayas (Figure 2a), we would predict a broadly distributed change in rock uplift rates at the surface without a sharp break from reset to unreset ages. As noted by *Brewer and Burbank* [2006], this structural geometry should produce a smooth increase in cooling ages from north to south, as the transport time from the closure isotherm increases toward the foreland. This scenario is broadly consistent with the trend reported by *Bollinger et al.* [2004] within the Kathmandu allochthon, but the presence

of unreset $^{40}\text{Ar}/^{39}\text{Ar}$ cooling ages in the LHS precludes such a structural configuration persisting in our study area over long timescales. If the HST ramp is instead presumed to merge into a surface breaking thrust (Figure 2c), all rocks to the north of this surface faulting should be reset, while all those to the south should remain unreset. This first-order result is insensitive to the overthrusting and underthrusting rates across the HST or thermal properties of the LHS and GHS rocks: Given sufficient time for rocks in the hanging wall to reach the surface, this geometry will create a break from reset to unreset cooling ages collocated with the break in rock uplift rates. In this case, a surface-breaking thrust provides a simple explanation for the collocation of changes in rock uplift rates, cooling ages, and physiography in central Nepal, consistent with the interpretations proposed by *Wobus et al.* [2003, 2005]. Because either of these end-member cases, surface thrusting or transport over a buried ramp, can be evaluated without a thermal model, we focus our modeling discussion on scenarios with nonzero accretion rates, as has been suggested by *Bollinger et al.* [2004].

5.1. Model Setup

[31] Our model is designed to provide a simplified representation of the Himalayan system that allows us to predict the pattern of reset and unreset cooling ages at the surface. In order to successfully predict these patterns, the key parameters for our model to estimate are (1) the position at which the 350°C closure isotherm intersects the HST ramp at depth and (2) the hanging wall particle trajectories from this position to the surface (Figure 7). Because we seek to describe only these parameters, our model setup is much simplified compared to previous efforts to describe the Himalayan system [*Henry et al.*, 1997; *Bollinger et al.*, 2006]. In particular, we have only a two-layer model, neglect shear heating, and restrict our model domain to the region surrounding the ramp in the HST. While a more complex representation of the model domain might allow more detailed predictions about thermal history of samples at the surface, our simplified model captures the most important parameters for predicting the patterns of reset and unreset samples at the surface. Furthermore, the simple framework described in our model can be easily exported to more complex parameterizations of material and kinematic properties.

[32] Our model domain is centered on the ramp in the HST, which we assume to dip northward at approximately 18° (similar to the geometry proposed by *Lave and Avouac* [2001] and *Avouac* [2003]). Our model grid is 100 km wide by 60 km deep, with a horizontal resolution of 1000 m and a vertical resolution of 325 m. Using this simplified geometry, the upper boundary of our model represents the elevation at the HST flat, which we assume to lie at a depth of ~5 km at the position of PT₂ (Figure 7). We use a constant temperature boundary condition at the top of the model domain for both the hanging wall and the footwall. In the footwall of the HST, we assign this upper boundary a temperature of 100°C; this relatively low temperature is chosen to approximately match the temperatures at this depth from existing thermal models [e.g., *Henry et al.*,

1997; *Brewer and Burbank*, 2006], and it is also consistent with what might be expected due to the presence of a cold Indian slab underthrusting along the HST [*Huerta et al.*, 1996]. In the hanging wall, we assign a higher temperature of 150°C at this upper boundary, to reflect the additional ~1.5 km of topography in the hanging wall of the HST. While these upper boundary conditions are clearly a simplification, we note that geologically reasonable changes in these boundary conditions do not significantly influence the geometry of the 350°C isotherm near the HST ramp, the model region of interest to us.

[33] The boundary conditions along the sides of the model are based on steady state one-dimensional (1-D) geotherms. Mantle heat flow is set at a constant value of 30 mW m⁻² at a depth of 100 km. Heat production is layered, with 15 km thick heat producing layers with radioactivity of 2.0 and 1.5 μW m⁻³ for the hanging wall and footwall of the HST, respectively. The lower layer is assigned a heat production of 1.0 μW m⁻³ in both the hanging wall and the footwall. All of the parameters used in our model are within the range of those estimated for the Himalaya and used in other thermal models of the range [e.g., *Rao et al.*, 1976; *Macfarlane*, 1992; *Huerta et al.*, 1996; *Henry et al.*, 1997; *Beaumont et al.*, 2001; *Bollinger et al.*, 2004]. In addition, our sensitivity analyses suggest that geologically reasonable variations in these values do not strongly affect the position of the 350°C closure isotherm where it intersects the HST ramp. As shown in Figure 7, this position is the most important contribution from the thermal modeling; combined with this constraint from the thermal model, the kinematics in the hanging wall then determine the position of the boundary between reset and unreset muscovites at the surface.

[34] The model employs a 2-D finite differencing algorithm, assuming a thermal diffusivity of $1 \times 10^{-6} \text{ m}^2 \text{ s}^{-1}$ and a thermal conductivity of 2.5 W m⁻¹ K⁻¹. For consistency with previous modeling efforts, fault-parallel convergence rates of 5 and 15 mm yr⁻¹ are used for the hanging wall overthrusting and footwall underthrusting rates, respectively [*Bollinger et al.*, 2004; *Brewer and Burbank*, 2006]. Initial model runs create a steady state thermal structure assuming that all advection in the hanging wall and footwall occurs parallel to the HST. This scenario may provide a reasonable simulation for the early evolution of the Himalaya prior to the development of PT₂, the Lesser Himalayan duplex, and structures farther south. The model thermally equilibrates to the prescribed convergence velocities after ~10 Myr, with a geometry of the closure isotherm similar to that observed in other thermal models for the Himalaya [*Huerta et al.*, 1996; *Henry et al.*, 1997; *Brewer and Burbank*, 2006]. This thermal structure is then exported to a model in which accretion is allowed to occur along the ramp in the HST.

[35] Once accretion is turned on, advection continues parallel to the fault while an additional component of advection is added across the fault to simulate underplating of material onto the hanging wall. We define the accretion rate in terms of the horizontal component of motion across the HST ramp. For computational efficiency, we do not

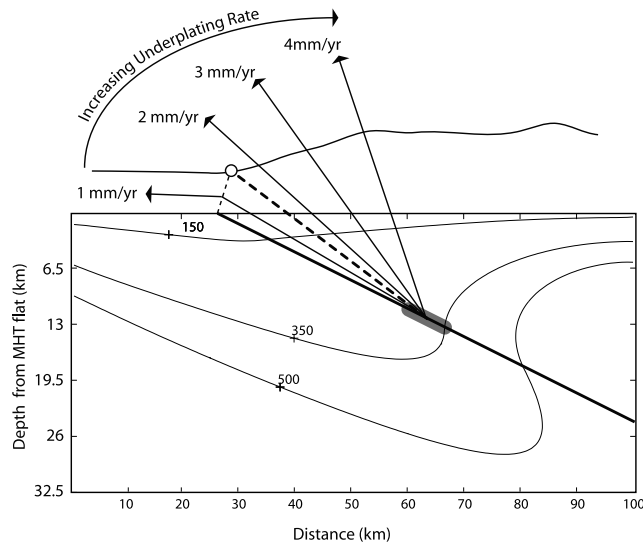


Figure 8. Position of cooling age break at the surface for varying underplating velocities. Grey shaded zone shows the range of intersection points between the 350°C isotherm and the HST ramp through all model runs. The 150°C , 350°C , and 500°C isotherms are shown for our initial steady state condition with overthrusting and underthrusting rates of 5 and 15 mm yr^{-1} , respectively, and no accretion (see text for description). Diagonal arrows show particle trajectories bounding reset and unreset ages for underplating velocities ranging from 1 to 4 mm yr^{-1} . For the parameters used in the model illustrated, the break in ages coincides with the physiographic transition for an underplating rate of $\sim 1.5\text{ mm yr}^{-1}$ (thick dashed line).

explicitly advect material properties (e.g., heat producing layers) across the zone of underplating. However, because the heat production values are similar between the LHS and the GHS, and because we do advect heat across this boundary, we do not expect this simplification to strongly affect the position of the 350°C closure isotherm. The most important effect of adding horizontal accretion to the model is therefore its influence on the kinematics in the hanging wall, which determines the particle paths from the closure isotherm to the surface. The intersection of the closure isotherm with the HST ramp is tracked through time, and the coevolving kinematic and thermal states are used to predict the distribution of reset and unreset cooling ages at the surface.

5.2. Model Results

[36] In our model of continuous accretion, particle paths in the hanging wall are a vector sum of the rate of accretion and the rate of fault-parallel overthrusting in the hanging wall (Figure 7). As the rate of accretion is increased, the break from reset to unreset cooling ages at the surface migrates northward; conversely, as the rate of accretion is decreased, the break in cooling ages migrates southward (Figure 8). Once the thermal state near the HST ramp has equilibrated, the position of the cooling age break at the

surface can therefore be easily determined by projecting a line from the intersection of the closure isotherm and the HST along a particle path defined by this simple vector sum. This constitutes an important kinematic difference from the model of Bollinger et al. [e.g., Bollinger et al., 2006] in which only continuity of the fault-normal component of the accretion vector is enforced. Accordingly, quantitative intercomparisons between models in terms of “accretion velocity” cannot be made. Both models, however, show similar responses to relative changes in modeled accretion velocities.

[37] Even with substantial thermal relaxation due to accretion of cold material from the footwall to the hanging wall, the intersection of the closure isotherm and the HST (marked “C” on Figure 7) does not vary significantly as the rate of accretion is changed. For a given set of thermal parameters (e.g., heat production, thickness of heat producing layers, diffusivity, thermal conductivity) and structural geometries (e.g., dip of HST ramp, position of accretion zone, depth of décollement at the position of the physiographic transition) we can therefore predict the position of the cooling age break at the surface within a relatively narrow range of uncertainty introduced by the thermal state in the upper crust.

[38] As an example, using the thermal parameters described above and assuming fault parallel overthrusting and underthrusting velocities of 5 and 15 mm yr^{-1} , respectively [Bollinger et al., 2004, 2006; Brewer and Burbank, 2006], we find that the cooling age break, uplift rate break, and physiographic transition coincide only for a horizontal accretion velocity of $\sim 1.5\text{ mm yr}^{-1}$ (Figure 8). In contrast, a model including out-of-sequence thrusting at the physiographic transition will reproduce this first-order observation for a wide range of kinematic conditions, since the fault itself represents a fundamental break in exhumation and cooling histories (see Figure 2b). Our thermokinematic modeling thus shows that continuous accretion and discrete surface faulting are both plausible mechanisms for producing the observed pattern of cooling ages in the central Himalaya, although very special circumstances are required for the continuous accretion scenario [e.g., Bollinger et al., 2004, 2006] to be viable.

6. Discussion

[39] The prominent discontinuity in cooling ages first observed in the Burhi Gandaki river [Copeland et al., 1991; Wobus et al., 2003] is also present in the Trisuli and Bhoté Kosi rivers, requiring a sharp northward increase in the total depth of exhumation along each of these transects. To first order, a tectonic model featuring out-of-sequence surface thrusting at the physiographic transition provides the simplest explanation for these distributions of cooling ages at the surface [e.g., Wobus et al., 2003, 2005]. Although it is not possible to rule out the alternative model of Bollinger et al. [2004, 2006] to explain these observations, we continue to favor the simpler model because it places fewer restrictions on the kinematics required to replicate the observed thermochronologic data. Regardless of the tectonic model

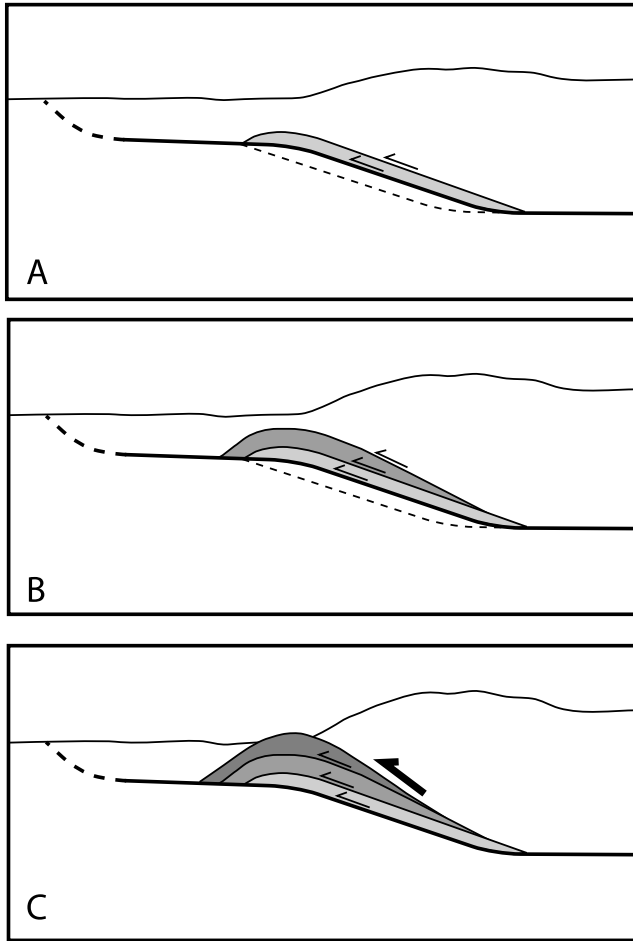


Figure 9. Schematic model for duplex evolution, following *Bollinger et al.* [2004]. (a–b) The duplex grows by addition of successive slivers of material from the footwall to the hanging wall (dashed lines), and the upper plate deforms by foliation-parallel shear. (c) Once surface erosion breaches the duplex, one of these roof thrusts may become a master fault localizing exhumation from the hanging wall directly to the surface.

invoked for any particular transect, however, the observed along-strike changes in surface structure, thermal history and physiography suggest substantial along-strike variations in the Pliocene-Quaternary structural evolution of central Nepal.

[40] We speculate that these along-strike changes reflect differences in the degree to which recent structures have developed along the physiographic transition in central Nepal. On one extreme, the presence of Tertiary $^{40}\text{Ar}/^{39}\text{Ar}$ ages throughout the Kathmandu allochthon, without a sharp discontinuity in cooling ages across the physiographic transition [*Bollinger et al.*, 2004], suggests that a sheet of deeply exhumed hanging wall rocks remains at the surface, and has not yet been breached by erosion. The broad synform preserved in the Kathmandu allochthon is consistent with duplexing at depth folding these rocks at the

surface. On the other extreme, sharp changes in physiography and cooling history in the Burhi Gandaki valley suggest the existence of a fully developed, surface-breaking thrust, whose morphologic expression continues eastward across the lower Trisuli river (Figure 3). Unreset $^{40}\text{Ar}/^{39}\text{Ar}$ cooling ages derived from LHS metasediments in the footwall of the Kathmandu thrust sheet suggest that if the Kathmandu thrust sheet was more extensive during early structural development of the Himalaya, it must have been thin enough that its immediate footwall remained below 350°C (see Figures 1 and 5).

[41] If our interpretations of the physiographic and thermochronologic data are correct, the along-strike differences in tectonic architecture may reflect varying stages of development in an evolving deformational pattern (Figure 9). The first stage may be characterized by duplexing and/or accretion along the basal ramp, in which penetrative foliation-parallel shear develops in the hanging wall to accommodate the added flux of material across the accretion zone [e.g., *Bollinger et al.*, 2004, 2006]. Eventually, focused erosion above the zone of accretion exposes one or more of these foliation-parallel shear zones at the surface. This surface-breaking thrust then becomes the primary locus of deformation, along which hanging wall overthrusting can be accommodated as a steady state structural configuration. The observed variations in physiography, cooling history, and structural geometry along the strike of the central Nepalese Himalaya suggest that we may be witnessing various stages of this structural evolution in different transects. For example, the tectonic “bridge” proposed to exist between the Kathmandu allochthon and the Greater Himalaya (e.g., Figure 1) is suggestive of an unbreached Greater Himalayan (i.e., MCT) thrust sheet (e.g., Figures 9a and 9b). To the east and west, Lesser Himalayan rocks remained at shallow structural levels prior to the development of a surface-breaking thrust that breached a growing duplex structure (e.g., Figure 9c).

[42] More subtle differences in the nature and position of the physiographic transition suggest differences in the role of preexisting structures such as the Main Central Thrust system in accommodating neotectonic displacements. In the Marsyandi valley, for example, the physiographic transition overlaps with the observed surface trace of the MCT system (compare Figures 4 and 5), and penetrative brittle deformation postdating Pliocene muscovite growth suggests Quaternary displacements within this zone [*Hodges et al.*, 2004]. In the Burhi Gandaki valley to the east, more abrupt changes in physiography are collocated with a break in cooling ages and erosion rates approximately 20 km south of the MCT system [*Wobus et al.*, 2003, 2005]. These observations favor a model including surface displacements on a newly developed thrust at PT₂, rather than a simple “reactivation” of a strand of the Main Central Thrust system. Similarly in the Trisuli valley, the sharp physiographic transition ~20 km south of the MCT system and the thermochronologic discontinuity farther north may suggest the development of multiple out-of-sequence thrusts over the Pliocene-Quaternary interval. Finally, relatively gradual changes in physiography in the Bhote Kosi transect imply a

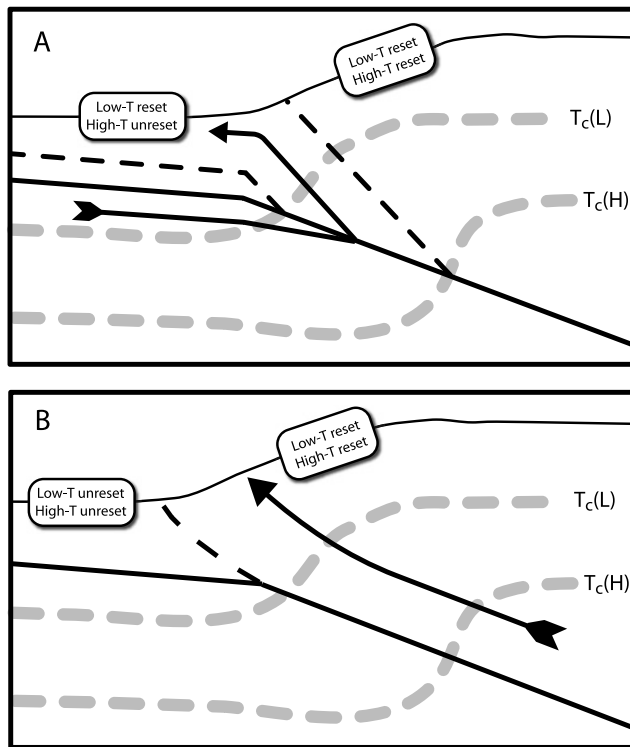


Figure 10. Simplified schematic diagrams showing the expected distribution of reset and unreset cooling ages at the surface for low-temperature and high-temperature thermochronometers under varying tectonic scenarios. Dashed grey lines show the closure isotherms, labeled $T_c(L)$ and $T_c(H)$, for low- and high-temperature thermochronometers, respectively. (a) If the physiographic transition results from accretion along the HST ramp, the kinematics should create a wide zone in which the low-T thermochronometer is reset but the high-T thermochronometer is not. (b) If the physiographic transition represents an active thrust, the break from reset to unreset ages should be approximately coincident for both thermochronometers.

zone of more broadly distributed strain, but the sharp break in $^{40}\text{Ar}/^{39}\text{Ar}$ cooling ages across this zone requires a substantial difference in exhumation history.

[43] Because our thermochronologic data are sensitive only to middle crustal temperatures, it is not possible to determine unambiguously that neotectonic out-of-sequence surface faulting is required in central Nepal, but additional low-temperature thermochronologic data (e.g., (U-Th)/He apatite and/or zircon) might help to resolve this issue. For example, the particle trajectories implied by an accretion model should create a zone of reset (U-Th)/He apatite ages at the surface in which the $^{40}\text{Ar}/^{39}\text{Ar}$ ages are not reset. This spatial offset between reset zones for different temperature thermochronometers would not be expected in a continuous surface thrusting architecture, since this geometry at steady state provides no mechanism of passing through the lower temperature closure isotherm without first passing through

the higher one (e.g., Figure 10). One good candidate for such a test would be the Ulleri augen gneiss in the Trisuli valley, a lithology which should yield apatite and zircon for low-temperature thermochronometry and whose $^{40}\text{Ar}/^{39}\text{Ar}$ ages and low metamorphic grade suggest it has remained at shallow structural levels throughout Himalayan evolution. The presence of reset (U-Th)/He ages in this unit would place additional constraints on its thermal evolution, and might suggest a history of shallow burial and exhumation consistent with an accretion model, rather than a protracted history at shallow structural levels as implied by a model of surface thrusting at PT_2 . In addition, low-temperature thermochronologic data on these rocks would help to resolve the cause of the observed offset between PT_2 and the reset/unreset $^{40}\text{Ar}/^{39}\text{Ar}$ cooling ages in the Trisuli transect.

7. Conclusions

[44] The sharp physiographic transition between the Lower and the Higher Himalaya in central Nepal is suggestive of spatial gradients in rock uplift rates over relatively short (~ 10 km) length scales. The general coincidence between this physiographic transition and a change from reset to unreset detrital $^{40}\text{Ar}/^{39}\text{Ar}$ dates in the Burhi Gandaki, Trisuli, and Bhote Kosi valleys suggests that these gradients in rock uplift have persisted at least long enough to preserve a prominent discontinuity in cooling history within the Lesser Himalayan Sequence. Our simple thermal and kinematic modeling does not rule out a model including accretion across the HST ramp, but suggests that only a narrow range of kinematic conditions can give rise to the collocation of physiographic and thermochronologic discontinuities in the absence of surface faulting. A simpler tectonic model which requires fewer constraints on the kinematics and structural geometry includes active, out-of-sequence thrust faulting where the physiographic transition is well expressed [e.g., *Wobus et al.*, 2003, 2005]. Along-strike changes in physiography and cooling history through central Nepal may reflect variability in structural style across length scales of less than 100 km, suggesting that both models may be applicable for different parts of the central Nepalese Himalaya.

[45] One of the variables that could influence the style of deformation is surface erosion. In an orogenic system with only weak or moderate erosion, accretion at depth may be the favored tectonic mode, passively uplifting the surface while allowing the orogen to widen toward the foreland. In contrast, vigorous erosion at the surface requires a mechanism of replenishing material from depth, favoring deeper exhumation within the zone of focused erosion and perhaps exploiting preexisting shear zones in a deforming hanging wall. The collocation of a zone of strong monsoon precipitation, a prominent physiographic transition, and a discontinuity in cooling history through much of central Nepal suggests that such a coupled system may have developed here. Continued vigorous erosion at the foot of the high Himalayas might be expected to breach remaining erosional outliers of hanging wall thrust sheets (e.g., the Kathmandu allochthon) with time, eventually allowing exhumation to

become concentrated along a single set of deformational structures throughout central Nepal.

[46] **Acknowledgments.** We thank Laurent Bollinger and an anonymous reviewer for constructive reviews that motivated significant improvements to the original manuscript. We also thank Bill Olszewski, Xifan

Zhang, and Malcolm Pringle for assistance in the laboratory and Leigh Royden for assistance with early modeling efforts. Field assistance from Ben Crosby, Kate Ruhl, Taylor Schildgen, Nicole Wobus, and Himalayan Experience Treks is gratefully acknowledged. Funding was provided by NSF Tectonics grant EAR-008758 to K.X.W. and K.V.H.

References

- Arita, K. (1983), Origin of the inverted metamorphism of the lower Himalayas, central Nepal, *Tectonophysics*, *95*, 43–60.
- Avouac, J. P. (2003), Mountain building, erosion and the seismic cycle in the Nepal Himalaya, *Adv. Geophys.*, *46*, doi:10.1016/S0065-2687(1003)46001-46009.
- Beaumont, C., R. A. Jamieson, M. H. Nguyen, and B. Lee (2001), Himalayan tectonics explained by extrusion of a low-viscosity crustal channel coupled to focused surface denudation, *Nature*, *414*, 738–742.
- Beaumont, C., R. A. Jamieson, M. H. Nguyen, and S. Medvedev (2004), Crustal channel flows: 1. Numerical models with applications to the tectonics of the Himalayan-Tibetan orogen, *J. Geophys. Res.*, *109*, B06406, doi:10.1029/2003JB002809.
- Bilham, R., K. Larson, J. Freymuller, and P. I. Members (1997), GPS measurements of present-day convergence across the Nepal Himalaya, *Nature*, *386*, 61–64.
- Bollinger, L., J. P. Avouac, O. Beyssac, E. J. Catlos, T. M. Harrison, M. Grove, B. Goffé, and S. Sapkota (2004), Thermal structure and exhumation history of the Lesser Himalaya in central Nepal, *Tectonics*, *23*, TC5015, doi:10.1029/2003TC001564.
- Bollinger, L., P. Henry, and J. P. Avouac (2006), Mountain building in the Nepal Himalaya: Thermal and kinematic model, *Earth Planet. Sci. Lett.*, *244*, 58–71.
- Brewer, I. D., and D. W. Burbank (2006), Thermal and kinematic modeling of bedrock and detrital cooling ages in the central Himalaya, *J. Geophys. Res.*, doi:10.1029/2004JB003304, in press.
- Brewer, I. D., D. W. Burbank, and K. V. Hodges (2003), Modeling detrital cooling-age populations: Insights from two Himalayan catchments, *Basin Res.*, *15*, 305–320.
- Burbank, D. W., A. E. Blythe, J. Putkonen, B. A. Pratt-Sitaula, E. J. Gabet, M. E. Oskin, A. P. Barros, and T. Ojha (2003), Decoupling of erosion and climate in the Himalaya, *Nature*, *426*, 652–655.
- Catlos, E. J., T. M. Harrison, M. J. Kohn, M. Grove, F. J. Ryerson, C. E. Manning, and B. N. Upreti (2001), Geochronologic and thermobarometric constraints on the evolution of the Main Central Thrust, central Nepal Himalaya, *J. Geophys. Res.*, *106*, 16,177–16,204.
- Cattin, R., and J. P. Avouac (2000), Modeling mountain building and the seismic cycle in the Himalaya of Nepal, *J. Geophys. Res.*, *105*, 13,389–13,407.
- Cattin, R., G. Martelet, P. Henry, J. P. Avouac, M. Diament, and T. R. Shakya (2001), Gravity anomalies, crustal structure and thermo-mechanical support of the Himalayas in central Nepal, *Geophys. J. Int.*, *147*, 381–392.
- Colchen, M., P. Le Fort, and A. Pecher (1986), *Recherches Géologiques dans l'Himalaya du Nepal, Annapurna-Manaslu-Ganesh Himal*, 136 pp., Centre Natl. de la Rech. Sci., Paris.
- Coleman, M. E. (1998), U-Pb constraints on Oligocene-Miocene deformation and anatexis within the central Himalaya, Marsyandi valley, Nepal, *Am. J. Sci.*, *298*, 553–571.
- Copeland, P., T. M. Harrison, K. V. Hodges, P. Maruejol, P. Le Fort, and A. Pecher (1991), An early Pliocene thermal disturbance of the Main Central Thrust, central Nepal: Implications for Himalayan tectonics, *J. Geophys. Res.*, *96*, 8475–8500.
- DeCelles, P. G., G. E. Gehrels, Q. J. B. LaReau, and M. Spurlin (2000), Tectonic implications of U-Pb zircon ages of the Himalayan Orogenic Belt in Nepal, *Science*, *288*, 497–499.
- DeCelles, P. G., D. M. Robinson, J. Quade, T. P. Ojha, C. N. Garzzone, P. Copeland, and B. N. Upreti (2001), Stratigraphy, structure, and tectonic evolution of the Himalayan fold-thrust belt in western Nepal, *Tectonics*, *20*, 487–509.
- Edwards, R. M. (1995), ⁴⁰Ar/³⁹Ar geochronology of the Main Central Thrust (MCT) region: Evidence for late Miocene to Pliocene disturbances along the MCT, Marsyangdi river valley, west-central Nepal Himalaya, *J. Nepal Geol. Soc.*, *10*, 41–46.
- Fielding, E., B. Isacks, M. Barazangi, and C. Duncan (1994), How flat is Tibet?, *Geology*, *22*, 163–167.
- Gehrels, G. E., P. G. DeCelles, A. Martin, T. P. Ojha, G. Pinhassi, and B. N. Upreti (2003), Initiation of the Himalayan orogen as an early Paleozoic thinned-thrust belt, *GSA Today*, *13*, 4–9.
- Harrison, T. M., F. J. Ryerson, P. Le Fort, A. Yin, O. Lovera, and E. J. Catlos (1997), A late Miocene–Pliocene orogen for the central Himalayan inverted metamorphism, *Earth Planet. Sci. Lett.*, *146*, E1–E7.
- Harrison, T. M., M. Grove, O. M. Lovera, and E. J. Catlos (1998), A model for the origin of Himalayan anatexis and inverted metamorphism, *J. Geophys. Res.*, *103*, 27,017–27,032.
- Hauck, M. L., K. D. Nelson, L. D. Brown, W. Zhao, and A. R. Ross (1998), Crustal structure of the Himalayan Orogen at approximately 90° east longitude from Project INDEPTH deep reflection profiles, *Tectonics*, *17*, 481–500.
- Heim, A., and A. Gansser (1939), Central Himalaya: Geological observations of Swiss expedition, 1936, *Mem. Soc. Helv. Sci. Nat.*, *73*, 1–245.
- Henry, P., X. Le Pichon, and B. Goffé (1997), Kinematic, thermal and petrological model of the Himalaya: Constraints related to metamorphism within the underthrust Indian crust and topographic elevation, *Tectonophysics*, *273*, 31–56.
- Hodges, K. V. (2000), Tectonics of the Himalaya and southern Tibet from two perspectives, *Geol. Soc. Am. Bull.*, *112*, 324–350.
- Hodges, K. (2003), Geochronology and thermochronology of orogenic systems, in *Treatise on Geochemistry: The Crust*, vol. 3, edited by R. L. Rudnick, pp. 263–292, Elsevier, New York.
- Hodges, K. V., J. M. Hurtado, and K. X. Whipple (2001), Southward extrusion of Tibetan crust and its effect on Himalayan tectonics, *Tectonics*, *20*, 799–809.
- Hodges, K., C. Wobus, K. Ruhl, T. Schildgen, and K. Whipple (2004), Quaternary deformation, river steepening and heavy precipitation at the front of the Higher Himalayan ranges, *Earth Planet. Sci. Lett.*, *220*, 379–389.
- Hodges, K. V., K. Ruhl, C. Wobus, and M. Pringle (2005), ⁴⁰Ar/³⁹Ar geochronology of detrital minerals, in *Low-Temperature Thermochronology: Techniques, Interpretations and Applications*, edited by P. W. Reiners and T. A. Ehlers, pp. 239–257, Mineral. Soc. of Am., Washington, D. C.
- Huerta, A. D., L. H. Royden, and K. V. Hodges (1996), The interdependence of deformational and thermal processes in mountain belts, *Science*, *273*, 637–639.
- Huntington, K. W., and K. V. Hodges (2006), A comparative study of detrital mineral and bedrock age-elevation methods for determining erosion rates, *J. Geophys. Res.*, doi:10.1029/2005JF000454, in press.
- Jackson, M., and R. Bilham (1994), Constraints on Himalayan deformation inferred from vertical velocity fields in Nepal and Tibet, *J. Geophys. Res.*, *99*, 13,897–13,912.
- Jamieson, R. A., C. Beaumont, S. Medvedev, and M. H. Nguyen (2004), Crustal channel flows: 2. Numerical models with implications for metamorphism in the Himalayan-Tibetan orogen, *J. Geophys. Res.*, *109*, B06407, doi:10.1029/2003JB002811.
- Johnson, M. R. W., G. J. H. Oliver, R. R. Parrish, and S. P. Johnson (2001), Synthrusting metamorphism, cooling, and erosion of the Himalayan Kathmandu Complex, Nepal, *Tectonics*, *20*, 394–415.
- Kirby, E., and K. X. Whipple (2001), Quantifying differential rock-uplift rates via stream profile analysis, *Geology*, *29*, 415–418.
- Kohn, M. J., E. J. Catlos, F. J. Ryerson, and T. M. Harrison (2001), Pressure-temperature-time path discontinuity in the Main Central thrust zone, central Nepal, *Geology*, *29*, 571–574.
- Koppers, A. P. (2002), ArArCALC software for ⁴⁰Ar/³⁹Ar age calculations, *Comput. Geosci.*, *28*, 605–619.
- Lague, D., A. Crave, and P. Davy (2003), Laboratory experiments simulating the geomorphic response to tectonic uplift, *J. Geophys. Res.*, *108*(B1), 2008, doi:10.1029/2002JB001785.
- Lave, J., and J. P. Avouac (2001), Fluvial incision and tectonic uplift across the Himalayas of central Nepal, *J. Geophys. Res.*, *106*, 26,561–26,591.
- Lyon-Caen, H., and P. Molnar (1983), Constraints on the structure of the Himalaya from an analysis of gravity anomalies and a flexural model of the lithosphere, *J. Geophys. Res.*, *88*, 8171–8191.
- Macfarlane, A. M. (1992), The Tectonic Evolution of the Core of the Himalaya, Langtang National Park, central Nepal, Ph.D. thesis, Mass. Inst. of Technol., Cambridge.
- Macfarlane, A., K. V. Hodges, and D. Lux (1992), A structural analysis of the Main Central thrust zone, Langtang National Park, central Nepal Himalaya, *Geol. Soc. Am. Bull.*, *104*, 1389–1402.
- Martin, A. J., P. G. DeCelles, G. E. Gehrels, P. J. Patchett, and C. Isachsen (2005), Isotopic and structural constraints on the location of the Main Central Thrust in the Annapurna Range, central Nepal Himalaya, *Geol. Soc. Am. Bull.*, *117*, 926–944.
- Molnar, P. (2003), Nature, nurture and landscape, *Nature*, *426*, 612–614.
- Pandey, M. R., R. P. Tandukar, J. P. Avouac, J. Lave, and J. P. Massot (1995), Interseismic strain accumulation on the Himalayan crustal ramp (Nepal), *Geophys. Res. Lett.*, *22*, 751–754.
- Pearson, O. N., and P. G. DeCelles (2005), Structural geology and regional tectonic significance of the Ramgarh thrust, Himalayan fold-thrust belt of Nepal, *Tectonics*, *24*, TC4008, doi:10.1029/2003TC001617.
- Rai, S. M. (2001), Geology, geochemistry and radiochronology of the Kathmandu and Gosainkund crystalline nappes, central Nepal Himalaya, *J. Nepal Geol. Soc.*, *25*, 135–155.
- Rai, S. M., S. Guillot, P. Le Fort, and B. N. Upreti (1998), Pressure-temperature evolution in the Kathmandu and Gosainkund regions, central Nepal, *J. Asian Earth Sci.*, *16*, 283–298.
- Rao, R. U. M., G. V. Rao, and H. Narain (1976), Radioactive heat generation and heat flow in the Indian shield, *Earth Planet. Sci. Lett.*, *30*, 57–64.

- Renne, P. R., C. C. Swisher, A. L. Deino, D. B. Kamber, T. L. Owens, and D. J. DePaolo (1998), Intercalibration of standards, absolute ages and uncertainties in $^{40}\text{Ar}/^{39}\text{Ar}$ dating, *Chem. Geol.*, *145*, 117–152.
- Robinson, D. M., P. G. DeCelles, C. N. Garzzone, O. N. Pearson, T. M. Harrison, and E. J. Catlos (2003), Kinematic model for the Main Central Thrust in Nepal, *Geology*, *31*, 359–362.
- Roe, G. H., D. R. Montgomery, and B. Hallet (2003), Orographic precipitation and the relief of mountain ranges, *J. Geophys. Res.*, *108*(B6), 2315, doi:10.1029/2001JB001521.
- Ruhl, K. W., and K. V. Hodges (2005), The use of detrital mineral cooling ages to evaluate steady state assumptions in active orogens: An example from the central Nepalese Himalaya, *Tectonics*, *24*, TC4015, doi:10.1029/2004TC001712.
- Schelling, D., and K. Arita (1991), Thrust tectonics, crustal shortening, and the structure of the far-eastern Nepal Himalaya, *Tectonics*, *10*, 851–862.
- Searle, M. P., R. R. Parrish, K. V. Hodges, A. Hurford, M. W. Ayres, and M. J. Whitehouse (1997), Shisha Pangma leucogranite, South Tibetan Himalaya: Field relations, geochemistry, age, origin, and emplacement, *J. Geol.*, *105*, 295–317.
- Seeber, L., and V. Gornitz (1983), River profiles along the Himalayan arc as indicators of active tectonics, *Tectonophysics*, *92*, 335–367.
- Shrestha, S. B., J. N. Shrestha, and S. R. Sharma (1987), Geological map of central Nepal, Nepal Dep. of Mines and Geol., Kathmandu, Nepal.
- Snyder, N., K. Whipple, G. Tucker, and D. Merritts (2000), Landscape response to tectonic forcing: DEM analysis of stream profiles in the Mendocino triple junction region, northern California, *Geol. Soc. Am. Bull.*, *112*, 1250–1263.
- Stöcklin, J. (1980), Geology of Nepal and its regional frame, *J. Geol. Soc. London*, *137*, 1–34.
- Thiede, R. C., B. Bookhagen, J. R. Arrowsmith, E. R. Sobel, and M. R. Strecker (2004), Climatic control on rapid exhumation along the southern Himalayan Front, *Earth Planet. Sci. Lett.*, *222*, 791–806.
- Upreti, B. N., and P. Le Fort (1999), Lesser Himalayan crystalline nappes of Nepal: Problems of their origin, in *Himalaya and Tibet: Mountain Roots to Mountain Tops*, edited by A. Macfarlane, R. B. Sorkhabi and J. Quade, *Spec. Pap. Geol. Soc. Am.*, *328*, 225–238.
- Vannay, J.-C., and K. Hodges (1996), Tectonometamorphic evolution of the Himalayan metamorphic core between Annapurna and Dhaulagiri, central Nepal, *J. Metamorph. Geol.*, *14*, 635–656.
- Vannay, J., B. Grasemann, M. Rahn, W. Frank, A. Carter, V. Baudraz, and M. Cosca (2004), Miocene to Holocene exhumation of metamorphic crustal wedges in the NW Himalaya: Evidence for tectonic extrusion coupled to fluvial erosion, *Tectonics*, *23*, TC1014, doi:10.1029/2002TC001429.
- Viskupic, K. M., K. V. Hodges, and S. A. Bowring (2005), Timescales of melt generation and the thermal evolution of the Himalayan metamorphic core, Everest region, eastern Nepal, *Contrib. Mineral. Petrol.*, *149*, 1–21.
- Whipple, K. X., and G. E. Tucker (1999), Dynamics of the stream-power river incision model: Implications for height limits of mountain ranges, landscape response timescales, and research needs, *J. Geophys. Res.*, *104*, 17,661–17,674.
- Whipple, K. X., and G. E. Tucker (2002), Implications of sediment-flux-dependent river incision models for landscape evolution, *J. Geophys. Res.*, *107*(B2), 2039, doi:10.1029/2000JB000044.
- Wobus, C. W., K. V. Hodges, and K. X. Whipple (2003), Has focused denudation sustained active thrusting at the Himalayan topographic front?, *Geology*, *31*, 861–864.
- Wobus, C., A. Heimsath, K. Whipple, and K. Hodges (2005), Active out-of-sequence thrust faulting in the central Nepalese Himalaya, *Nature*, *434*, 1008–1011.
- Wobus, C., K. Whipple, E. Kirby, N. Snyder, J. Johnson, K. Spyropolou, B. T. Crosby, and D. Sheehan (2006), Tectonics from topography: Procedures, promise and pitfalls, in *Tectonics, Climate and Landscape Evolution: Penrose Conference Series*, edited by S. D. Willett et al., *Spec. Pap. Geol. Soc. Am.*, *398*, 55–74.
- Zhao, W., K. D. Nelson, J. Che, J. Quo, D. Lu, C. Wu, and X. Liu (1993), Deep seismic reflection evidence for continental underthrusting beneath southern Tibet, *Nature*, *366*, 557–559.

K. V. Hodges and K. X. Whipple, Department of Earth, Atmospheric and Planetary Sciences, Massachusetts Institute of Technology, Cambridge, MA 02139, USA.

C. W. Wobus, CIRES, University of Colorado, Campus Box 216, Boulder, CO 80309. (cameron.wobus@colorado.edu)